

CoDA: Exploring Chain-of-Distribution Attacks and Post-Hoc Token-Space Repair for Medical Vision-Language Models

Xiang Chen, Fangfang Yang, Chunlei Meng, Chengyin Hu, Ang Li, Yiwei Wei, Jiahuan Long, Jiujiang Guo

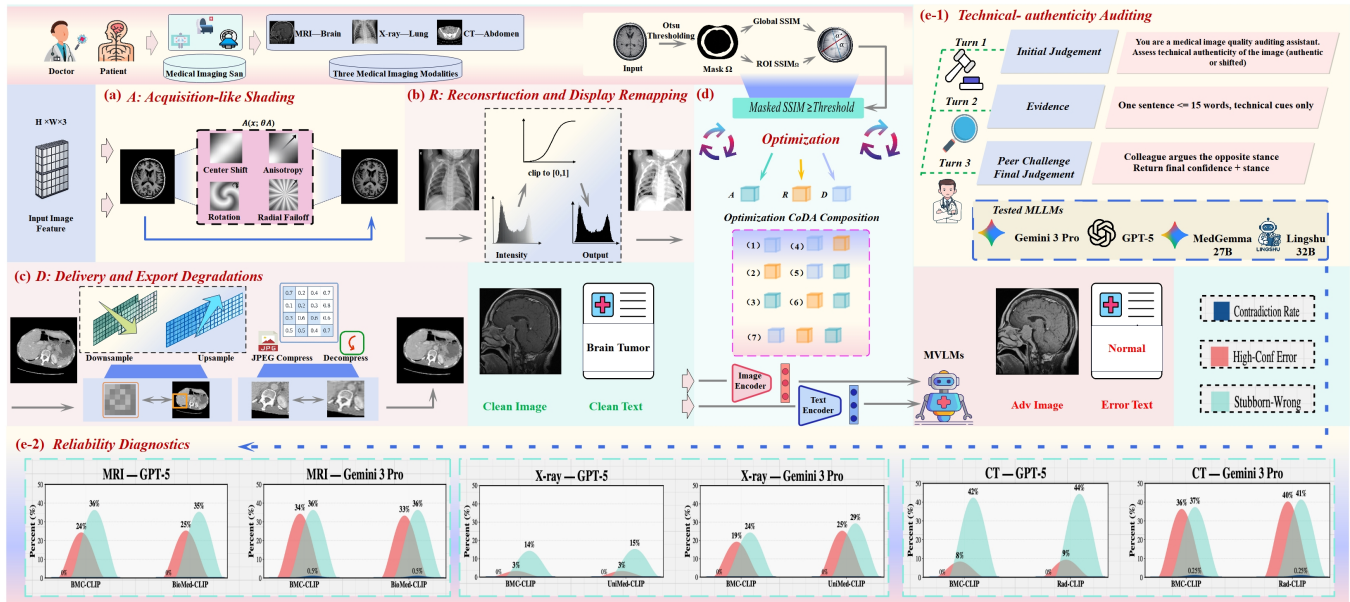


Figure 1: Overview of CoDA. (a-c) Three pipeline stages: acquisition-like shading (A), reconstruction and display remapping (R), and delivery and export degradations (D), illustrated on brain MRI, chest X-ray, and abdominal CT. (d) CoDA optimizes over seven stage compositions and within-stage parameters under masked similarity constraints to produce visually plausible adversarial samples. (e-1-e-2) Technical-authenticity auditing and reliability diagnostics.

Abstract

Medical vision-language models (MVLMs) are increasingly used as perceptual backbones in radiology pipelines and as the visual front end of multimodal assistants, yet their reliability under real clinical imaging workflows remains underexplored. Prior robustness evaluations often assume clean, curated inputs or study isolated corruptions and pixel-level perturbations, overlooking routine acquisition, reconstruction, display, and delivery operations that preserve clinical readability while subtly shifting image statistics. To address this gap, we propose CoDA, a chain-of-distribution framework that constructs clinically plausible pipeline shifts by composing acquisition-like shading, reconstruction and display remapping, and delivery and export degradations. Under masked structural-similarity constraints, CoDA jointly optimizes stage-composition families and within-stage parameters to induce failures while preserving visual plausibility. Across brain MRI, chest X-ray, and abdominal CT, CoDA substantially degrades the zero-shot performance of CLIP-style MVLMs, with ablations showing that chained compositions are consistently more damaging than any single stage. We also evaluate multimodal large language models (MLLMs) as technical-authenticity auditors of imaging realism and quality rather than pathology. Proprietary multimodal models

show degraded auditing reliability and persistent high-confidence errors on CoDA-shifted samples under a single-call self-challenge protocol, while the medical-specific MLLMs we test exhibit clear deficiencies in medical image quality auditing. Finally, we introduce a post-hoc repair strategy based on teacher-guided token-space adaptation with patch-level alignment, which improves accuracy on archived CoDA outputs. Overall, our findings characterize a clinically grounded threat surface for MVLm deployment and show that lightweight alignment improves robustness in deployment.

CCS Concepts

• **Computing methodologies** → **Computer vision**; Machine learning; • **Security and privacy** → *Systems security*.

Keywords

Robustness and security evaluations, CoDA, Post-hoc repair strategy

1 Introduction

MVLMs are increasingly adopted as general-purpose perceptual backbones in radiology AI, enabling zero-shot recognition and retrieval, report-aware representation learning, and language-guided

visual grounding. Their progress has been driven by contrastive pretraining and domain-specific adaptation, including CLIP-style vision–language pretraining [29], medical image–text contrastive learning [43], report-based radiology representation learning [45], and large-scale biomedical figure–caption pretraining [42]. Specialized CLIP variants for radiology and expanding biomedical archives have further improved medical encoders [23, 24], while visually instructed MLLMs are emerging in parallel as multimodal assistants [10, 22, 28]. Since the vision encoder governs visual evidence for downstream reasoning, front-end robustness is safety-critical.

Clinical images, however, rarely arrive as pristine tensors. They are shaped by imaging workflows in which acquisition conditions affect intensity profiles, reconstruction and display settings remap physical measurements to pixels (e.g., window and level in DICOM viewers) [26], and delivery operations such as resampling and compression introduce systematic artifacts [5]. These steps usually preserve human interpretability, yet they can alter low-level statistics in ways that MVLM representations may depend on. More broadly, distribution shift is known to degrade deployed models [9, 16, 27, 35, 41], and recent robustness benchmarks for large vision–language models show that routine, non-malicious perturbations can induce substantial failures even when semantics remain intact [3, 4, 31, 34, 39, 44]. Nevertheless, robustness evaluations for MVLMs still often emphasize clean public datasets or isolated perturbations, leaving limited coverage of multi-stage variability introduced by real clinical pipelines.

We address this gap with an adversarial yet clinically grounded threat model. Rather than considering classic norm-bounded pixel attacks, we study an attacker who manipulates plausible pipeline operations and their parameters through realistic acquisition, reconstruction, and delivery processes. We propose CoDA, a chain-of-distribution attack that composes three stages: acquisition-like shading, reconstruction and display remapping, and delivery and export degradations. Under masked structural-similarity constraints that preserve visual plausibility [37], CoDA optimizes failure-inducing parameterizations over both composition families and within-stage parameters. This design reflects clinical workflows in which deviations accumulate across multiple processing steps and interact under realistic clinical operating conditions.

Using CoDA, we show that chained pipeline shifts substantially undermine zero-shot CLIP-style MVLMs across brain MRI, chest X-ray, and abdominal CT. Ablations restricting the shift space to individual stages confirm that chained compositions are consistently more damaging than any single-stage variant under the same plausibility constraints. We then examine whether MLLM-based multimodal assistants can serve as a safety layer by auditing technical authenticity, assessing imaging realism and quality rather than pathology. Motivated by evidence that MLLMs can hallucinate visual content and remain confidently wrong [13, 20], we adapt reliability diagnostics to the medical pipeline setting and evaluate these auditors under CoDA-shifted inputs. This setting is particularly challenging because the induced shifts remain visually plausible while perturbing the technical cues that auditing-oriented systems are expected to detect. We find that several strong proprietary assistants behave reliably on clean inputs yet fail to consistently flag adversarial pipeline outputs, even under self-challenge-style prompting [36, 38]. We further find that the medical-specific MLLMs

we evaluate exhibit clear deficiencies in medical image quality auditing, limiting their utility as a quality-control layer under realistic clinical pipeline variability.

We further investigate a lightweight post-hoc repair strategy to improve robustness without full retraining. The design combines parameter-efficient adaptation methods such as LoRA and SSF [15, 40] with ideas from knowledge distillation [12], efficient visual adaptation [14, 25], and recent robustness-oriented adaptation for vision–language models [7, 21]. Specifically, we introduce a teacher-guided token-space adaptation scheme that aligns a student vision encoder with the token structure of a stronger teacher while preserving the student’s interface and computational profile. Evaluated on archived CoDA outputs, this repair improves MVLM zero-shot classification accuracy, suggesting that post-hoc alignment can recover performance under clinically plausible deployment-time pipeline shifts. We summarize our main contributions as follows:

- We propose CoDA, a clinically grounded attack space that composes acquisition-like shading, reconstruction and display remapping, and delivery and export degradations, and optimizes both the stage composition and the stage parameters under masked similarity constraints.
- We conduct a multi-stage robustness evaluation of CLIP-style MVLMs on brain MRI, chest X-ray, and abdominal CT, including controlled ablations that isolate each stage and budget analyses that quantify how attack strength scales with optimization iterations.
- We show that CoDA degrades zero-shot MVLM performance and weakens technical authenticity auditing by multimodal assistants under realistic pipeline shifts. We further show that lightweight teacher-guided token-space repair can recover robustness without full retraining, while remaining compatible with practical deployment requirements in clinical workflows.

2 Related Work

2.1 Robustness and Distribution Shift

Recent work on robustness increasingly emphasizes structured perturbations and realistic distribution shifts, rather than synthetic worst-case noise alone. In multimodal and vision–language settings, robustness degrades under adversarial attacks [31, 39, 44], as well as under compositional shifts, spurious correlations, and changing evaluation settings [3, 4, 16, 34, 35]. This perspective is especially relevant for real-world clinical deployment, where images may undergo acquisition variability, reconstruction changes, export artifacts, and other workflow-induced transformations while remaining clinically interpretable and diagnostically usable. Our work follows this line by targeting clinically plausible multi-stage pipeline variability across acquisition, reconstruction, and delivery processes in realistic medical imaging workflows.

2.2 Medical Vision–Language Pretraining

Medical vision–language models extend CLIP-style contrastive learning by leveraging paired reports, biomedical captions, and large-scale medical corpora to acquire transferable representations for zero-shot transfer and cross-task generalization in radiology [23,

Table 1: Attack success rate (%). Each entry gives the success rate after optimizing the within-family parameters for its CoDA composition family. Bold indicates the best within each modality block (MRI/X-ray/CT) for the same model and setting.

Model	Setting	MRI						X-ray						CT								
		A	R	D	A+R	R+D	A+D	A+R+D	A	R	D	A+R	R+D	A+D	A+R+D	A	R	D	A+R	R+D	A+D	A+R+D
BioMed-CLIP	Random ($\tau = 0.90$)	11	40	33	35	54	26	38	71	61	75	33	45	75	24	69	73	67	66	68	67	74
	Random ($\tau = 0.80$)	22	61	17	52	62	25	44	75	77	100	53	63	67	61	69	88	50	70	81	75	76
	Bayes ($\tau = 0.90$)	0	61	25	45	58	7	45	69	68	90	44	42	100	37	62	76	60	64	68	87	79
	Bayes ($\tau = 0.80$)	0	51	100	61	47	45	68	73	73	90	70	85	100	78	71	76	54	70	92	94	79
UniMed-CLIP	Random ($\tau = 0.90$)	83	21	71	19	48	80	50	0	19	96	6	100	100	50	76	86	67	84	76	79	90
	Random ($\tau = 0.80$)	67	26	69	37	47	83	59	0	23	97	15	100	91	40	89	87	81	90	97	92	71
	Bayes ($\tau = 0.90$)	75	31	79	23	35	66	68	0	33	95	11	94	100	75	80	92	68	91	89	88	86
	Bayes ($\tau = 0.80$)	67	27	70	41	57	73	74	9	29	97	22	95	80	64	90	91	88	91	97	91	89
BMC-CLIP	Random ($\tau = 0.90$)	0	42	47	33	54	20	42	0	19	96	6	100	100	50	80	83	29	77	56	21	50
	Random ($\tau = 0.80$)	0	47	45	42	49	47	38	0	23	97	15	100	91	40	78	83	30	72	59	18	45
	Bayes ($\tau = 0.90$)	0	30	47	33	50	40	48	0	33	95	11	94	100	75	83	84	37	69	48	23	37
	Bayes ($\tau = 0.80$)	0	39	47	33	60	27	52	9	29	97	22	95	80	64	83	90	21	66	45	33	49
Rad-CLIP	Random ($\tau = 0.90$)	73	16	100	20	27	33	15	-	50	50	85	36	20	67	100	45	32	69	42	53	71
	Random ($\tau = 0.80$)	58	29	100	48	36	79	45	-	58	50	88	57	43	81	94	88	61	80	45	61	58
	Bayes ($\tau = 0.90$)	56	15	50	34	27	62	23	0	52	50	87	33	25	77	82	57	38	66	49	53	62
	Bayes ($\tau = 0.80$)	67	38	-	50	50	64	59	-	61	71	91	44	0	85	100	90	50	82	55	69	69

24, 42, 43, 45]. These advances have substantially broadened the practical scope of medical vision–language pretraining across recognition and retrieval tasks in diverse radiological settings and institutions worldwide. However, deployment reliability remains shaped by heterogeneity in scanners, acquisition protocols, reconstruction settings, and downstream processing, where small yet systematic variations can alter pixel statistics without compromising clinical interpretability. Prior medical AI studies have shown that dataset bias and shortcut features can inflate benchmark performance while degrading generalization under real-world shift [9, 41]. Complementing this line of work, we study pipeline-consistent shift spaces that stress-test MVLMS under clinically plausible variability and show how compounded stages can expose vulnerabilities often missed by standard single-stage evaluations in prior robustness studies of medical imaging systems.

2.3 Multimodal Reliability and Security

Multimodal assistants expand the threat surface beyond pixel robustness to the broader image–language interface. In medical settings, reliability can be compromised by prompt injection [8], jail-break and cross-modality mismatch behaviors [17], backdoor vulnerabilities in medical image–text models [18], and model stealing under adversarial domain alignment [33]. These studies indicate that safe clinical deployment depends on the stability of the full image–language interface, not visual robustness alone. A related but less explored question is whether multimodal models can act as technical safeguards by auditing image realism and acquisition quality. Our results further show that this capability is itself fragile under clinically plausible chained shifts: proprietary multimodal models degrade on CoDA outputs, while the evaluated medical-specific MLLMs exhibit little reliable medical image quality auditing capability under these challenging conditions.

3 Methodology

3.1 Problem Definition

We study CLIP-style MVLMS consisting of an image encoder f_{img} and a text encoder f_{text} [29]. Given an image $x \in \mathbb{R}^{H \times W \times 3}$, we use the ℓ_2 -normalized image embedding:

$$z(x) = \frac{f_{img}(x)}{\|f_{img}(x)\|_2} \in \mathbb{R}^d \quad (1)$$

For zero-shot classification evaluation, we follow prompt ensembling [29]. For each class $c \in \{0, 1\}$ with prompt set \mathcal{T}_c , we construct the corresponding class prototype representation:

$$t_c = \frac{1}{|\mathcal{T}_c|} \sum_{t \in \mathcal{T}_c} \frac{f_{text}(t)}{\|f_{text}(t)\|_2} \in \mathbb{R}^d \quad (2)$$

We score classes by cosine similarity $s_c(x) = \langle z(x), t_c \rangle$ and define the margin as $m(x) = s_1(x) - s_0(x)$. Given label $y \in \{0, 1\}$, we use a signed correctness score:

$$J(x, y) = m(x) \cdot \sigma(y) \quad \sigma(y) = \begin{cases} +1, & y = 1 \\ -1, & y = 0 \end{cases} \quad (3)$$

where $\sigma(\cdot)$ maps the binary label to ± 1 , so that $J(x, y) < 0$ indicates a prediction flip.

3.2 CoDA Shift Space and Compositions

CoDA models pipeline variability using three parameterized stages: acquisition-like shading (A), reconstruction and display remapping (R), and delivery and export degradations (D). For the transformations below, we assume an intensity-normalized input image, denote $x \in [0, 1]^{H \times W \times 3}$, and use $\text{clip}(\cdot)$ to clamp values to $[0, 1]$.

Stage A (Acquisition-like Shading). We apply a smooth multiplicative gain field $M_A(\cdot; \theta_A) \in \mathbb{R}^{H \times W}$ to model acquisition-induced,

Table 2: Zero-shot accuracy (%). Clean vs. CoDA-shifted performance for CLIP-style MVLMS across modalities. Parentheses denote the absolute drop from the clean baseline for Bayesian optimization with $\tau = 0.8$.

Setting	BioMed-CLIP			UniMed-CLIP			BMC-CLIP			Rad-CLIP		
	MRI	X-ray	CT	MRI	X-ray	CT	MRI	X-ray	CT	MRI	X-ray	CT
Clean	81.5	64.0	57.5	65.0	58.5	54.0	78.5	50.5	54.0	93.0	85.5	50.0
$\tau = 0.9$ / Random	62.5	52.5	31.0	51.5	51.0	21.0	62.0	40.5	44.0	76.0	37.0	44.5
$\tau = 0.8$ / Random	50.5	32.0	25.0	47.5	46.5	11.5	57.5	38.0	42.5	56.5	31.5	33.0
$\tau = 0.9$ / Bayes	56.5	45.5	29.0	48.0	48.5	15.5	59.5	38.0	44.5	71.5	33.5	44.0
$\tau = 0.8$ / Bayes	44.0	24.5	22.0	44.0	42.5	8.5	57.0	32.5	40.0	50.5	28.0	30.0

spatially varying intensity gains (e.g., center shift, anisotropy, rotation, and radial falloff) in routine clinical imaging. Fig. 1(a) shows representative examples of this effect:

$$A(x; \theta_A) = \text{clip}(x \odot M_A(x; \theta_A)) \quad (4)$$

Here, \odot denotes element-wise multiplication broadcast over channels, and θ_A collects the gain strength and geometric parameters that define M_A .

Stage R (Reconstruction and Display Remapping). To capture reconstruction and viewing variability, we apply robust window-level normalization followed by a monotone tone curve, gamma adjustment, and bit-depth quantization. These steps mirror common clinical viewing and conversion toolchains [26], with qualitative illustrations provided in Fig. 1(b):

$$R(x; \theta_R) = Q_b \left(T \left(\text{clip} \left(\frac{x - c}{w + \varepsilon} + \frac{1}{2} \right) \right)^y \right) \quad (5)$$

Here, (c, w) are the window center and width computed from robust quantiles of a grayscale proxy and then adjusted by offsets (Δ_c, s_w) , ε is a small constant for numerical stability, $T(\cdot)$ is a piecewise-linear monotone tone curve defined by control points $(0, 0)$, $(0.25, y_{25})$, $(0.5, y_{50})$, $(0.75, y_{75})$, and $(1, 1)$ with monotonicity enforced, and $Q_b(\cdot)$ denotes b -bit uniform quantization. We denote $\theta_R = \{\Delta_c, s_w, y_{25}, y_{50}, y_{75}, \gamma, b\}$.

Stage D (Delivery and Export Degradations). We model delivery-time artifacts using downsample-upsample resizing $\mathcal{S}_\rho(\cdot)$ and compression-induced degradation $\mathcal{J}_q(\cdot)$, which together approximate common export and transmission artifacts in clinical image pipelines [5]. The resulting degradations are shown in Fig. 1(c):

$$D(x; \theta_D) = \mathcal{J}_q(\mathcal{S}_\rho(x)) \quad (6)$$

Here, $\rho \in (0, 1]$ is the resize factor, q is the compression-quality factor, and $\theta_D = \{q, \rho\}$.

Compositions. CoDA evaluates seven composition families under the canonical stage order $A \rightarrow R \rightarrow D$:

$$\mathcal{F} = \{A, R, D, A \circ R, R \circ D, A \circ D, A \circ R \circ D\} \quad (7)$$

For a family $F \in \mathcal{F}$ with parameters θ , we denote the shifted candidate by $x_{\text{shift}} = F(x; \theta)$, where θ bundles the relevant subsets of $(\theta_A, \theta_R, \theta_D)$ required by the chosen family.

To preserve visual plausibility, we enforce structural similarity (SSIM) [37] constraints both globally and within a foreground region of interest (ROI). Specifically, we derive a binary ROI mask $\Omega(x) \in \{0, 1\}^{H \times W}$ from the input image using threshold-based foreground extraction [2], which separates the dominant anatomical

foreground from background areas. For local patches u and v , SSIM is defined as:

$$\text{SSIM}(u, v) = \frac{(2\mu_u\mu_v + C_1)(2\sigma_{uv} + C_2)}{(\mu_u^2 + \mu_v^2 + C_1)(\sigma_u^2 + \sigma_v^2 + C_2)} \quad (8)$$

We compute $\text{SSIM}(x, x')$ by averaging the SSIM map over all pixels, and $\text{SSIM}_\Omega(x, x')$ by averaging only over pixels where $\Omega(x) = 1$, providing a foreground-sensitive assessment that emphasizes clinically relevant structures:

$$\text{SSIM}(x, x_{\text{shift}}) \geq \tau, \text{SSIM}_\Omega(x, x_{\text{shift}}) \geq \tau \quad (9)$$

When x_{shift} violates the constraints, we project it into the feasible set by mixing:

$$x_\alpha = (1 - \alpha)x + \alpha x_{\text{shift}} \quad \alpha \in [0, 1] \quad (10)$$

Here x_α is the mixed sample and α controls the perturbation strength. We choose the largest feasible mixing coefficient via:

$$\alpha^* = \arg \max_{\alpha \in [0, 1]} \alpha \quad \text{s.t.} \quad \text{SSIM}(x, x_\alpha) \geq \tau, \text{SSIM}_\Omega(x, x_\alpha) \geq \tau \quad (11)$$

and denote the final constrained sample by $x_{\text{adv}} = x_{\alpha^*}$.

3.3 Optimization and Family Selection

Let $x_{\text{adv}}(x; F, \theta, \tau)$ denote the constrained output obtained by applying family F with parameters θ to x , followed by α -projection under threshold τ . For each image-label pair (x, y) , family $F \in \mathcal{F}$, and threshold τ , we optimize the within-family parameters to minimize signed correctness after projection, as illustrated in Fig. 1(d):

$$\theta^{(F)} = \arg \min_{\theta \in \mathcal{S}_F} J(x_{\text{adv}}(x; F, \theta, \tau), y) \quad (12)$$

where \mathcal{S}_F denotes the admissible parameter domain for family F . This formulation allows each family to be optimized within its own clinically plausible parameter range while treating the underlying model as a black box. It also decouples optimization over composition families from that over stage-specific parameters, enabling CoDA to capture both structural and parametric failure sources in realistic imaging workflows, where small deviations across stages may accumulate and interact nonlinearly. This separation allows CoDA to distinguish failures driven by stage composition from those caused by stage-wise parameter sensitivity within the same family. We optimize the objective using random search and TPE-based Bayesian optimization in Optuna [1].

After obtaining $\theta^{(F)}$ for each family, we select the final adversarial output from the family yielding the lowest signed correctness

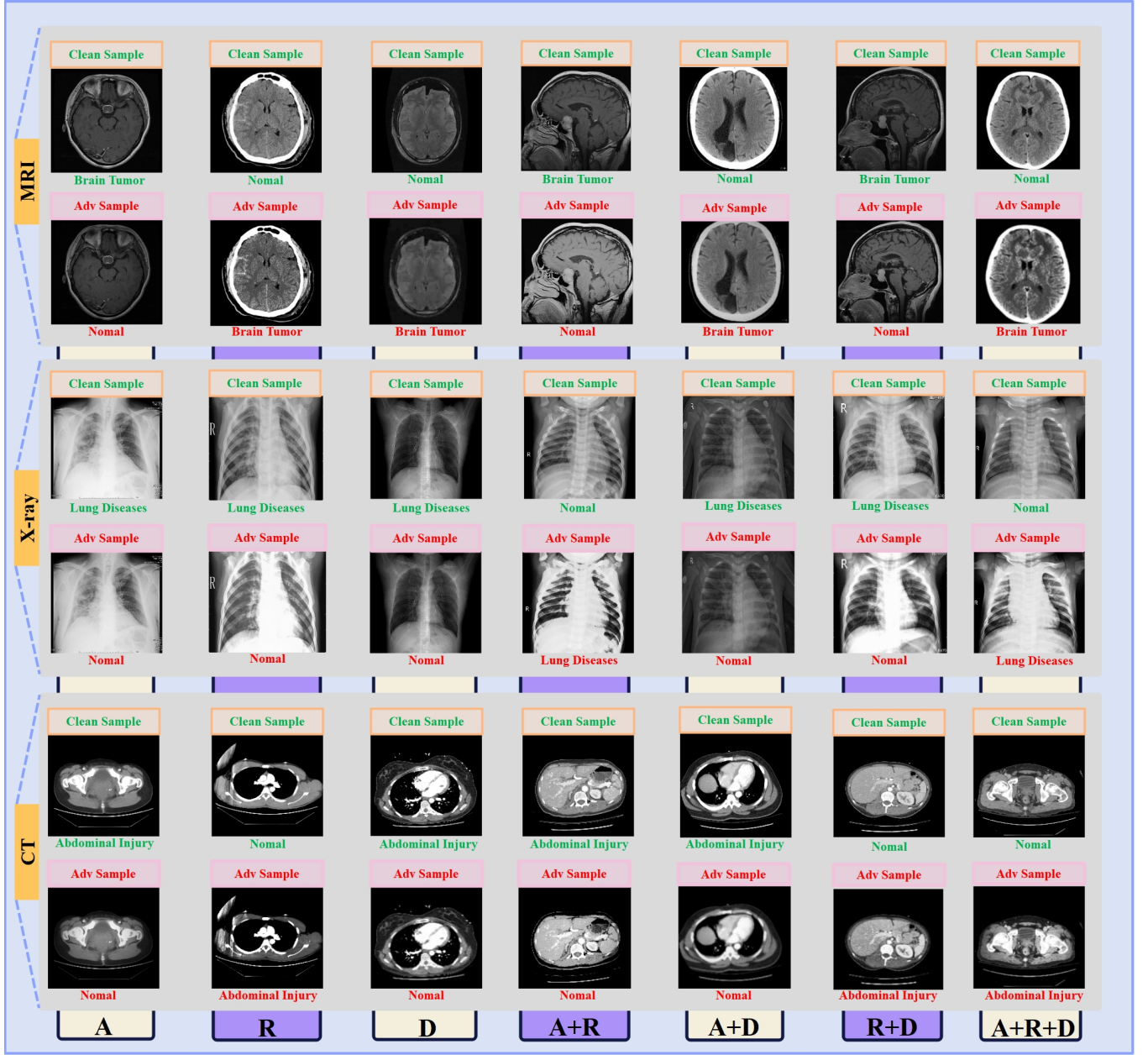


Figure 2: Qualitative visualization of CoDA composition families. Representative clean and adversarial samples for MRI, X-ray, and CT under the CoDA shift space in Eq. 7.

across all candidates:

$$F^* = \arg \min_{F \in \mathcal{F}} J(x_{adv}(x; F, \theta^{(F)}, \tau), y) \quad (13)$$

3.4 Post-hoc Repair via Teacher-Guided Token-Space Adaptation

To mitigate failures without full retraining, we adapt a frozen student encoder with a lightweight residual token-space adapter, drawing on ideas from parameter-efficient adaptation methods such as

LoRA and SSF [15, 40], as well as knowledge distillation [12] and efficient visual adaptation [14, 25].

The overall repair workflow is summarized in Fig. 4(a). Let $T_S(x) \in \mathbb{R}^{(1+N) \times d}$ denote the student's post-layer-norm token sequence, where token index 0 is the CLS token and the remaining N tokens correspond to image patches. We insert a token-wise residual linear adapter:

$$\tilde{T}_S(x) = T_S(x) + T_S(x)W^T, \quad W \in \mathbb{R}^{d \times d} \quad (14)$$

Table 3: Ablation under Bayesian optimization ($\tau = 0.8$). Zero-shot accuracy (%) under single-stage shifts (Only A/Only R/Only D) versus the full chained CoDA shift (A+R+D).

Attack	BioMed-CLIP			UniMed-CLIP			BMC-CLIP			Rad-CLIP		
	MRI	X-ray	CT	MRI	X-ray	CT	MRI	X-ray	CT	MRI	X-ray	CT
Only A	75.5	61.0	47.5	62.0	56.5	44.0	77.0	48.0	63.0	73.0	68.0	46.0
Only R	57.0	33.0	31.0	56.0	49.0	31.5	61.5	41.5	48.0	56.5	40.0	35.0
Only D	76.5	60.5	40.5	56.0	52.5	37.5	69.5	42.0	58.0	65.0	52.0	39.0
CoDA	44.0	24.5	22.0	44.0	42.5	8.5	57.0	32.5	40.0	50.5	28.0	30.0

Here W is the only trainable parameter, while the student backbone remains frozen throughout.

Let $P_S(x) \in \mathbb{R}^{N \times d}$ denote the patch tokens extracted from $T_S(x)$ after excluding the CLS token, and let $\tilde{P}_S(x)$ denote the corresponding patch tokens extracted from $\tilde{T}_S(x)$ for alignment. A teacher encoder provides patch tokens $P_T(x)$; when the teacher and student token dimensions differ, we apply a fixed projection to obtain projected teacher tokens $P'_T(x)$ in the student token space.

We define a token-geometry operator through the normalized Gram matrix of patch tokens:

$$\mathcal{G}(P) = \text{norm}(P) \text{norm}(P)^\top \in \mathbb{R}^{N \times N} \quad (15)$$

where $\text{norm}(\cdot)$ row-normalizes tokens to unit ℓ_2 norm.

We train W on clean images with three components: (i) a task loss \mathcal{L}_{task} that preserves the original downstream objective, (ii) a view-consistency term weighted by λ_{cons} that encourages invariant margins across two mild workflow-inspired augmentations, and (iii) an optional teacher-guided geometry alignment weighted by λ_{dist} that matches the student and teacher patch-token similarity structure. The total objective is:

$$\mathcal{L} = \mathcal{L}_{task} + \lambda_{cons} (m(x^{(1)}) - m(x^{(2)}))^2 + \lambda_{dist} \|\mathcal{G}(\tilde{P}_S(x)) - \mathcal{G}(P'_T(x))\|_F^2 \quad (16)$$

Here $\|\cdot\|_F$ denotes the Frobenius norm. We evaluate repair directly on archived CoDA outputs without regenerating attacks.

4 Experiments

4.1 Experimental Settings

Datasets. We evaluate three imaging modalities using publicly available datasets spanning distinct anatomical regions. For brain MRI and chest X-ray, we follow the data organization protocol of Cheng et al. [6], which curates public source collections for robustness evaluation. For abdominal CT, we use the RSNA Abdominal Traumatic Injury CT (RATIC) dataset [30]. For each modality, we construct a balanced clean evaluation set with 100 positive and 100 negative images to isolate robustness effects under distribution shift [16, 34, 35].

Threat models. We evaluate CoDA under two plausibility thresholds, $\tau \in \{0.90, 0.80\}$, over the seven composition families in Eq. 7. For each image, the final adversarial output is obtained by constrained optimization with subsequent winner-family selection (Eq. 13). The evaluation covers three complementary target settings. Zero-shot robustness is assessed on a diverse set of medical vision-language models, namely BioMed-CLIP [42], UniMed-CLIP, BMC-CLIP [23], and Rad-CLIP [24]. Technical-authenticity

auditing is conducted on proprietary multimodal assistants from the OpenAI GPT family [28] and the Google Gemini family [10, 11], alongside medical-specific MLLMs including Lingshu [19] and MedGemma [32]. For post-hoc robustness repair, we select modality-specific teacher-student pairs according to attacked performance in the zero-shot setting and train a token-space adapter (Eq. 14) with the objective in Eq. 16. Specifically, BMC-CLIP is used as the teacher for MRI and CT, whereas UniMed-CLIP is used for X-ray; the student models are Rad-CLIP for MRI and X-ray, and UniMed-CLIP for CT. Repair performance is measured directly on archived CoDA outputs without regenerating adversarial samples.

Baseline methods. For classification, we report clean accuracy and performance under CoDA at two plausibility thresholds, $\tau \in \{0.90, 0.80\}$. For each τ , we optimize CoDA using both random search and Bayesian optimization, and report the resulting zero-shot accuracy. For technical-authenticity auditing, we evaluate all auditors on clean inputs and on CoDA-shifted images generated by Bayesian optimization at $\tau = 0.80$. For post-hoc repair, we compare a token-space adapter trained without teacher guidance against a teacher-guided variant with patch-token geometry alignment [12, 14, 25] to improve robustness in deployment.

Implementation. Constrained optimization is performed using random search and TPE-based Bayesian optimization in Optuna [1]. For zero-shot classification, we evaluate brain MRI, chest X-ray, and abdominal CT in a binary disease-presence setting, using four semantically similar prompts for the positive and negative classes of each modality to reduce prompt sensitivity; full prompt sets are given in the appendix. For technical-authenticity auditing, we adopt a single-call self-challenge protocol inspired by consistency-based prompting [36, 38], and report accuracy and reliability diagnostics; full MLLM interaction details are provided in the appendix. For post-hoc repair, the adapter is trained only on clean images and tested directly on archived CoDA outputs without regenerating attacks, with $\lambda_{dist} = 1$ and $\lambda_{cons} = 0.1$ by default.

4.2 Zero-shot Classification Evaluation

We evaluate zero-shot classification on clean and CoDA-shifted inputs across MRI, X-ray, and CT. Table 1 reports the attack success rate of each composition family after optimizing within-family CoDA parameters for every modality-model pair. CoDA achieves high success rates across all modalities, with X-ray showing the greatest vulnerability: for several models, distortion-involved families approach or reach perfect success. MRI and CT exhibit a similar trend, although the strongest family is more model-dependent,

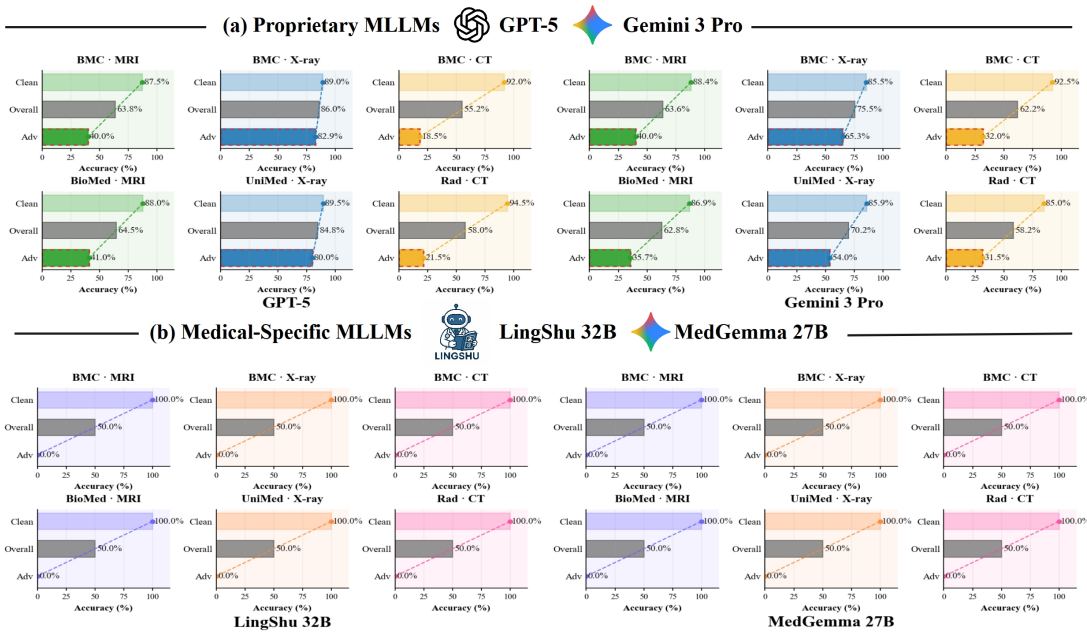


Figure 3: Auditing performance under clean vs. CoDA shifts. We compare proprietary and medical-specific MLLMs across MRI, X-ray, and CT, reporting clean accuracy, overall accuracy, and accuracy on CoDA-shifted inputs.

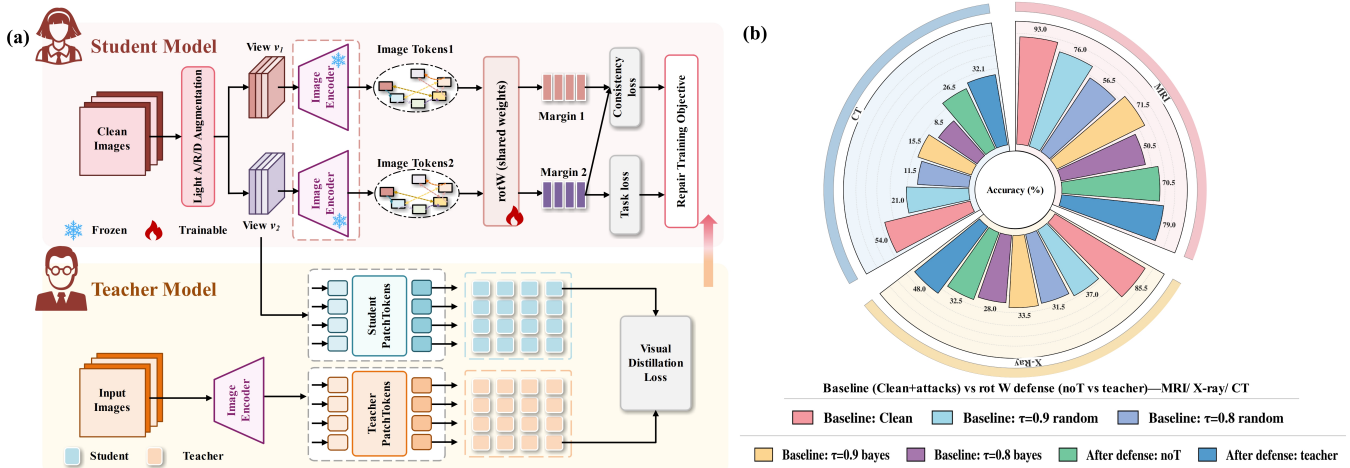


Figure 4: Post-hoc token-space repair. (a) A frozen teacher optionally guides a lightweight student token adapter (rotW) trained on clean data with task, view-consistency, and distillation losses. (b) Accuracy on archived CoDA outputs for the baseline and repaired models, comparing unguided vs. teacher-guided adaptation across MRI, CT, and X-ray.

suggesting that CoDA induces failures through multiple plausible pipeline variants rather than a single dominant transformation. Table 2 reports Top-1 accuracy (%) under clean inputs and different CoDA settings, including random and Bayesian optimization with $\tau \in \{0.90, 0.80\}$. Across all models and modalities, CoDA substantially degrades accuracy relative to the clean baseline, and Bayesian optimization is generally more effective than random optimization. These results show that clinically plausible pipeline shifts are sufficient to consistently disrupt zero-shot recognition in CLIP-style MVLMs, with X-ray and CT often exhibiting the largest degradation.

Fig. 2 shows representative clean and adversarial examples under the seven composition families in Eq. 7; although the perturbations largely preserve clinical readability, they introduce systematic appearance changes that are sufficient to alter or flip zero-shot predictions across modalities.

4.3 Technical Authenticity Auditing Evaluation

We evaluate multimodal assistants as technical-authenticity auditors. This non-clinical task asks whether an input image is a

plausible product of clinical acquisition and delivery, without assessing pathology. We study both proprietary multimodal model families [10, 11, 28] and medical-specific MLLMs [19, 32]. We use a single-call protocol that emulates three interaction stages: an initial judgment with confidence, one sentence of technical evidence, and a symmetric peer challenge before the final decision, as shown in Fig. 1(e-1). Beyond accuracy, we assess reliability using three indicators in Fig. 1(e-2): contradiction rate, high-confidence error, and stubborn-wrong behavior. Results show a clear split between model groups. Proprietary multimodal models remain relatively reliable on clean inputs, but their performance degrades markedly on CoDA-shifted samples, with persistent high-confidence errors despite the built-in self-challenge step. In contrast, the medical-specific MLLMs exhibit severe deficiencies in technical-authenticity auditing. As shown in Fig. 3, their accuracy falls to 0 on CoDA-shifted MRI, X-ray, and CT images, indicating a complete failure to judge whether such inputs remain technically plausible for real-world clinical acquisition. Taken together, these findings suggest that current medical-domain specialization alone is insufficient for reliable authenticity auditing under distribution shift.

4.4 Post-hoc Token-Space Repair Evaluation

We evaluate whether CoDA-induced failures can be mitigated without full retraining. For each modality, we adapt the student encoder using the residual token-space adapter in Eq. 14, optionally enhanced with a stronger teacher through patch-token geometry alignment. Training uses only clean images, while evaluation is performed directly on archived CoDA outputs to reflect practical deployment constraints. Fig. 4(b) compares the baseline student with the repaired variants on MRI, CT, and X-ray. The results show that token-space repair consistently improves robustness on adversarial inputs across all modalities, and that teacher-guided repair yields larger gains than the student-only variant. Nevertheless, a clear gap to clean performance remains, especially on X-ray and CT, indicating that lightweight post-hoc adaptation can partially but not fully recover CoDA-induced failures.

4.5 Ablation Study

Ablation of Optimization Iterations. We vary the iteration budget used by the constrained optimization routine and quantify how attack effectiveness scales with additional optimization steps. Fig. 5 reports the attack success rate as a function of iteration count for MRI, X-ray, and CT across four CLIP-style MVLMs. Increasing the budget consistently improves success, while gains taper after moderate iteration counts, indicating that most improvements can be achieved within the masked-SSIM feasible set.

Ablation of Single-Stage Shifts vs. Full CoDA ($\tau = 0.8$). To isolate the contribution of each pipeline component, we restrict the shift space to a single stage (Only A, Only R, or Only D) and compare against the full chained composition under the same plausibility threshold. Table 3 reports the resulting accuracies. Across models and modalities, the chained composition remains the most damaging setting, supporting the hypothesis that cross-stage interactions amplify brittleness beyond what any single stage induces.

Ablation of Repair Hyperparameters. We ablate two key hyperparameters in post-hoc token-space repair: the view-consistency

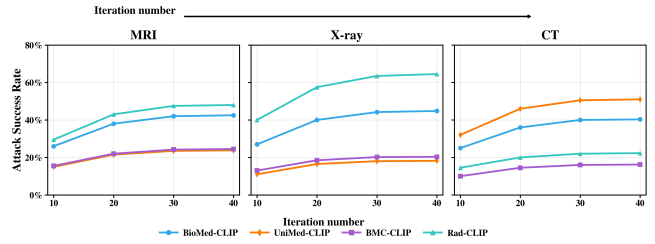


Figure 5: Ablation of optimization iterations. Attack success rate under CoDA as a function of the optimization iteration budget, reported for MRI, X-ray, and CT across BioMed-CLIP, UniMed-CLIP, BMC-CLIP, and Rad-CLIP.

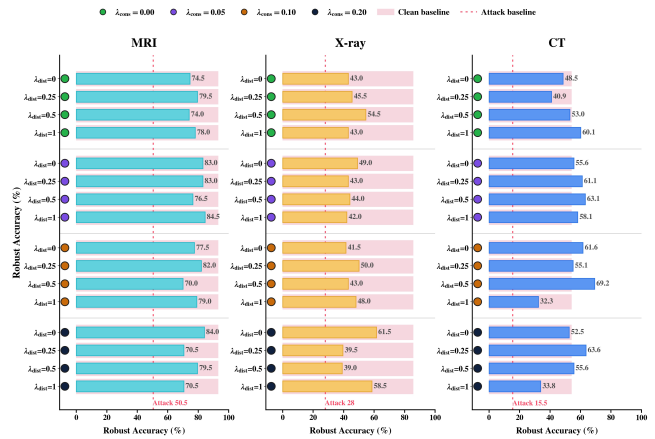


Figure 6: Ablation of repair hyperparameters. Robust accuracy under CoDA shifts as a function of λ_{cons} and λ_{dist} , compared against the clean baseline (gray) and the attack baseline (red dashed), reported for MRI/X-ray/CT.

weight λ_{cons} and the teacher-guidance weight λ_{dist} in Eq. 16. Fig. 6 shows that, across modalities, post-repair accuracy under CoDA-shifted inputs generally lies between the clean and attack baselines, exceeding the latter in most cases. In a few CT settings, the repaired model slightly outperforms the clean baseline, possibly because the student model itself shows relatively weak performance under clean baseline conditions in practice.

5 Conclusion

We propose CoDA, a chain-of-distribution framework that composes clinically plausible pipeline shifts and optimizations for failure-inducing parameterizations under masked similarity constraints. Across MRI, CT, and X-ray, CoDA substantially degrades the zero-shot performance of CLIP-style MVLMs and exposes fragility missed by single-stage testing. Multimodal assistants used as technical authenticity auditors can also fail under these shifts, including persistent high-confidence errors. A lightweight post-hoc repair via teacher-guided token-space adaptation partially restores robustness when evaluated directly on archived CoDA adversarial outputs.

References

- [1] Takuya Akiba, Shotaro Sano, Toshihiko Yanase, Takeru Ohta, and Masanori Koyama. 2019. Optuna: A Next-generation Hyperparameter Optimization Framework. In *Proceedings of the 25th ACM SIGKDD International Conference on Knowledge Discovery & Data Mining*. 2623–2631.
- [2] Mohammad Amiriebrahimabadi, Zhina Rouhi, and Najme Mansouri. 2024. A Comprehensive Survey of Multi-Level Thresholding Segmentation Methods for Image Processing. *Archives of Computational Methods in Engineering* 31 (2024), 3647–3697.
- [3] Rishika Bhagwatkar, Perampalli Shraavan Nayak, Reza Bayat, Alexis Roger, Daniel Z. Kaplan, Pouya Bashivan, and Irina Rish. 2024. Towards Adversarially Robust Vision-Language Models: Insights from Design Choices and Prompt Formatting Techniques. In *Proceedings of the 41st International Conference on Machine Learning*.
- [4] Rishika Bhagwatkar, Shraavan Nayak, Pouya Bashivan, and Irina Rish. 2024. Improving Adversarial Robustness in Vision-Language Models with Architecture and Prompt Design. In *Findings of the Association for Computational Linguistics: EMNLP 2024*. Association for Computational Linguistics, 17003–17020.
- [5] Nour El Houda Bourai, Hayet Farida Merouani, and Akila Djebbar. 2024. Deep Learning-Assisted Medical Image Compression Challenges and Opportunities: Systematic Review. *Neural Computing and Applications* 36 (2024), 10067–10108.
- [6] Zijie Cheng, Ariel Yuhang Ong, Siegfried K. Wagner, David A. Merle, Lie Ju, Hanyuan Zhang, Ruinian Chen, Linze Pang, Boxuan Li, Tiantian He, Anran Ran, Hongyang Jiang, Dawei Gabriel Yang, Ke Zou, et al. 2025. Understanding the Robustness of Vision-Language Models to Medical Image Artefacts. *npj Digital Medicine* 8 (2025), 727.
- [7] Wonjeong Choi, Sejong Ryu, Jungmoon Lee, Dong-Jun Han, and Jaekyun Moon. 2026. Identifying Robust Neural Pathways: Few-Shot Adversarial Mask Tuning for Vision-Language Models. In *International Conference on Learning Representations*.
- [8] Jan Clusmann, Dyke Ferber, Isabella C. Wiest, Carolin V. Schneider, Titus J. Brinker, Sebastian Foersch, Daniel Truhn, and Jakob Nikolas Kather. 2025. Prompt Injection Attacks on Vision Language Models in Oncology. *Nature Communications* 16 (2025), 1239.
- [9] Alex J. DeGrave, Joseph D. Janizek, and Su-In Lee. 2021. AI for Radiographic COVID-19 Detection Selects Shortcuts over Signal. *Nature Machine Intelligence* (2021).
- [10] Gemini Team. 2023. Gemini: A Family of Highly Capable Multimodal Models. *arXiv preprint arXiv:2312.11805* (2023).
- [11] Google DeepMind. 2024. Gemini 1.5: Unlocking Multimodal Understanding across Millions of Tokens of Context. *arXiv preprint arXiv:2403.05530* (2024).
- [12] Jianping Gou, Baosheng Yu, Stephen John Maybank, and Dacheng Tao. 2021. Knowledge Distillation: A Survey. *International Journal of Computer Vision* 129, 6 (2021), 1789–1819.
- [13] Tianrui Guan, Fuxiao Liu, Xiyang Wu, Ruiqi Xian, Zongxia Li, Xiaoyu Liu, Xijun Wang, Lichang Chen, Furong Huang, Yaser Yacoub, Dinesh Manocha, and Tianyi Zhou. 2024. HallusionBench: An Advanced Diagnostic Suite for Entangled Language Hallucination and Visual Illusion in Large Vision-Language Models. In *Proceedings of the IEEE/CVF Conference on Computer Vision and Pattern Recognition*. 14375–14385.
- [14] Haoyu He, Jianfei Cai, Jing Zhang, Dacheng Tao, and Bohan Zhuang. 2023. Sensitivity-Aware Visual Parameter-Efficient Fine-Tuning. In *Proceedings of the IEEE/CVF International Conference on Computer Vision*.
- [15] Edward J. Hu, Yelong Shen, Phillip Wallis, Zeyuan Allen-Zhu, Yuanzhi Li, Shean Wang, and Weizhu Chen. 2021. LoRA: Low-Rank Adaptation of Large Language Models. *arXiv preprint arXiv:2106.09685* (2021).
- [16] Chengyue Huang, Brisa Maneechotesuwarn, Shivang Chopra, and Zsolt Kira. 2025. FRAMES-VQA: Benchmarking Fine-Tuning Robustness across Multi-Modal Shifts in Visual Question Answering. In *Proceedings of the IEEE/CVF Conference on Computer Vision and Pattern Recognition*. 3909–3918.
- [17] Xijie Huang, Xinyuan Wang, Hantao Zhang, Yinghao Zhu, Jiawen Xi, Jingkun An, Hao Wang, Hao Liang, and Chengwei Pan. 2025. Medical MLLM Is Vulnerable: Cross-Modality Jailbreak and Mismatched Attacks on Medical Multimodal Large Language Models. In *Proceedings of the AAAI Conference on Artificial Intelligence*, Vol. 39. 3797–3805.
- [18] Ruinan Jin, Chun-Yin Huang, Chenyu You, and Xiaoxiao Li. 2024. Backdoor Attack on Unpaired Medical Image-Text Foundation Models: A Pilot Study on MedCLIP. *arXiv preprint arXiv:2401.01911* (2024).
- [19] LASA Team, Weiwen Xu, Hou Pong Chan, Long Li, Mahani Aljunied, Ruifeng Yuan, Jianyu Wang, Chenghao Xiao, Guizhen Chen, Chaoqun Liu, Zhaodonghui Li, Yu Sun, Junao Shen, Chaojun Wang, Jie Tan, Deli Zhao, Tingyang Xu, Hao Zhang, and Yu Rong. 2025. Lingshu: A Generalist Foundation Model for Unified Multimodal Medical Understanding and Reasoning. *arXiv preprint arXiv:2506.07044* (2025).
- [20] Yifan Li, Yifan Du, Kun Zhou, Jinpeng Wang, Wayne Xin Zhao, and Ji-Rong Wen. 2023. Evaluating Object Hallucination in Large Vision-Language Models. In *Proceedings of the 2023 Conference on Empirical Methods in Natural Language Processing*.
- [21] Chaohu Liu, Gui Tianyi, Yu Liu, and Linli Xu. 2026. AdPO: Enhancing the Adversarial Robustness of Large Vision-Language Models with Preference Optimization. In *International Conference on Learning Representations*.
- [22] Haotian Liu, Chunyuan Li, Qingyang Wu, and Yong Jae Lee. 2023. Visual Instruction Tuning. In *Advances in Neural Information Processing Systems*.
- [23] Alejandro Lozano, Min Woo Sun, Ivan Lopez, Jeffrey Gu, Jeffrey J. Nirschl, Josiah Aklilu, Anita Rau, Austin Wolfgang Katzer, Yuhui Zhang, James Burgess, Liangyu Chen, Collin Chiu, Xiaohan Wang, Alfred Seunghoon Song, Robert Tibshirani, and Serena Yeung-Levy. 2025. BIOMEDICA: An Open Biomedical Image-Caption Archive, Dataset, and Vision-Language Models Derived from Scientific Literature. In *Proceedings of the IEEE/CVF Conference on Computer Vision and Pattern Recognition*. 19724–19735.
- [24] Zhixiu Lu, Hailong Li, Nehal A. Parikh, Jonathan R. Dillman, and Lili He. 2024. RadCLIP: Enhancing Radiologic Image Analysis through Contrastive Language-Image Pre-training. *arXiv preprint arXiv:2403.09948* (2024).
- [25] Otniel-Bogdan Mercea, Alexey Gritsenko, Cordelia Schmid, and Anurag Arnab. 2024. Time-, Memory- and Parameter-Efficient Visual Adaptation. In *Proceedings of the IEEE/CVF Conference on Computer Vision and Pattern Recognition*.
- [26] National Electrical Manufacturers Association. 2024. Digital Imaging and Communications in Medicine (DICOM) Standard, PS3.3: Information Object Definitions. Standard.
- [27] Fahimeh Hosseini Noohdani, Parsa Hosseini, Aryan Yazdan Parast, Hamidreza Yaghoubi Araghi, and Mahdieh Soleymani Baghshah. 2024. Decompose-and-Compose: A Compositional Approach to Mitigating Spurious Correlation. In *Proceedings of the IEEE/CVF Conference on Computer Vision and Pattern Recognition*. 27662–27671.
- [28] OpenAI. 2023. GPT-4 Technical Report. *arXiv preprint arXiv:2303.08774* (2023).
- [29] Alec Radford, Jong Wook Kim, Chris Hallacy, Aditya Ramesh, Gabriel Goh, Sandhini Agarwal, Girish Sastry, Amanda Askell, Pamela Mishkin, Jack Clark, Gretchen Krueger, and Ilya Sutskever. 2021. Learning Transferable Visual Models From Natural Language Supervision. In *Proceedings of the 38th International Conference on Machine Learning (Proceedings of Machine Learning Research, Vol. 139)*. 8748–8763.
- [30] Jeffrey D. Rudie, Hui-Ming Lin, Robyn L. Ball, Sabeena Jalal, Luciano M. Prevedello, Savvas Nicolaou, Brett S. Marinelli, Adam E. Flanders, Kirti Magudia, George Shih, Melissa A. Davis, John Mongan, Peter D. Chang, Ferco H. Berger, Sebastiaan Hermans, Meng Law, Tyler Richards, Jan-Peter Grunz, Andreas Steven Kunz, Shobhit Mathur, Sandro Galea-Soler, Andrew D. Chung, Saif Afat, Chin-Chi Kuo, Layal Aweidah, Ana Villanueva Campos, Arjuna Somasundaram, Felipe Antonio Sanchez Tijmes, Attaporn Jantarangkoon, Leonardo Kayat Bittencourt, Michael Brassil, Ayoub El Hajjami, Hakan Dogan, Muris Becircic, Agrahara G. Bharatkumar, Eduardo Moreno J dice de Mattos Farina, and Errol Colak. 2024. The RSNA Abdominal Traumatic Injury CT (RATIC) Dataset. *Radiology: Artificial Intelligence* 6, 6 (2024), e240101.
- [31] Christian Schlarmann, Naman Deep Singh, Francesco Croce, and Matthias Hein. 2024. Robust CLIP: Unsupervised Adversarial Fine-Tuning of Vision Embeddings for Robust Large Vision-Language Models. In *Proceedings of the 41st International Conference on Machine Learning (Proceedings of Machine Learning Research, Vol. 235)*. 43685–43704.
- [32] Andrew Sellergren, Sahar Kazemzadeh, Tiam Jaroensri, Atilla Kiraly, Madeleine Traverse, Timo Kohlberger, Shawn Xu, Fayaz Jamil, Cian Hughes, Charles Lau, Justin Chen, Fereshteh Mahvar, Liron Yatziv, Tiffany Chen, Bram Sterling, Stefanie Anna Baby, Susanna Maria Baby, Jeremy Lai, Samuel Schmidgall, Lin Yang, et al. 2025. MedGemma Technical Report. *arXiv preprint arXiv:2507.05201* (2025).
- [33] Yaling Shen, Zhixiong Zhuang, Kun Yuan, Maria-Irina Nicolae, Nassir Navab, Nicolas Padoy, and Mario Fritz. 2025. Medical Multimodal Model Stealing Attacks via Adversarial Domain Alignment. In *Proceedings of the AAAI Conference on Artificial Intelligence*, Vol. 39. 6842–6850.
- [34] Haoqin Tu, Chenhang Cui, Zijun Wang, Yiyang Zhou, Bingchen Zhao, Junlin Han, Wangchunshu Zhou, Huaxiu Yao, and Cihang Xie. 2025. How Many Are in This Image? A Safety Evaluation Benchmark for Vision LLMs. In *Computer Vision – ECCV 2024 (Lecture Notes in Computer Science, Vol. 15109)*. 37–55.
- [35] Maya Varma, Jean-Benoit Delbrouck, Zhihong Chen, Akshay Chaudhari, and Curtis Langlotz. 2024. RaVL: Discovering and Mitigating Spurious Correlations in Fine-Tuned Vision-Language Models. In *Advances in Neural Information Processing Systems*.
- [36] Xuezhi Wang, Jason Wei, Dale Schuurmans, Quoc Le, Ed H. Chi, Sharan Narang, Aakanksha Chowdhery, and Denny Zhou. 2023. Self-Consistency Improves Chain of Thought Reasoning in Language Models. In *International Conference on Learning Representations*.
- [37] Zhou Wang, Alan C. Bovik, Hamid R. Sheikh, and Eero P. Simoncelli. 2004. Image Quality Assessment: From Error Visibility to Structural Similarity. *IEEE Transactions on Image Processing* 13, 4 (2004), 600–612.
- [38] Jason Wei, Xuezhi Wang, Dale Schuurmans, Maarten Bosma, Brian Ichter, Fei Xia, Ed H. Chi, Quoc V. Le, and Denny Zhou. 2022. Chain-of-Thought Prompting Elicits Reasoning in Large Language Models. In *Advances in Neural Information Processing Systems*.

- [39] Peng Xie, Yequan Bie, Jianda Mao, Yangqiu Song, Yang Wang, Hao Chen, and Kani Chen. 2025. Chain of Attack: On the Robustness of Vision-Language Models Against Transfer-Based Adversarial Attacks. In *Proceedings of the IEEE/CVF Conference on Computer Vision and Pattern Recognition*. 14679–14689.
- [40] Yiheng Xiong, Xinyu Zhang, Zhaoyang Wang, Yiqi Liu, and Qi Tian. 2022. Scaling and Shifting Your Features: A New Baseline for Efficient Model Tuning. *arXiv preprint arXiv:2210.08823* (2022).
- [41] John R. Zech, Marcus A. Badgeley, Ming Liu, Adam B. Costa, Joseph J. Titano, and Eric K. Oermann. 2018. Variable Generalization Performance of a Deep Learning Model to Detect Pneumonia in Chest Radiographs: A Cross-sectional Study. *PLOS Medicine* 15, 11 (2018), e1002683.
- [42] Sheng Zhang, Yanbo Xu, Naoto Usuyama, Hanwen Xu, Jaspreet Bagga, Robert Tinn, Sam Preston, Rajesh Rao, Mu Wei, Naveen Valluri, Cliff Wong, Andrea Tupini, Yu Wang, Matt Mazzola, Swadheen Shukla, Lars Liden, Jianfeng Gao, Angela Crabtree, Brian Piening, Carlo Bifulco, Matthew P. Lungren, Tristan Naumann, Sheng Wang, and Hoifung Poon. 2023. BiomedCLIP: A Multimodal Biomedical Foundation Model Pretrained from Fifteen Million Scientific Image-Text Pairs. *arXiv preprint arXiv:2303.00915* (2023).
- [43] Yuhao Zhang, Hang Jiang, Yasuhide Miura, Christopher D. Manning, and Curtis P. Langlotz. 2022. Contrastive Learning of Medical Visual Representations from Paired Images and Text. In *Proceedings of the Machine Learning for Healthcare Conference (Proceedings of Machine Learning Research, Vol. 182)*. 1–24.
- [44] Yunqing Zhao, Tianyu Pang, Chao Du, Xiao Yang, Chongxuan Li, Ngai-Man Cheung, and Min Lin. 2023. On Evaluating Adversarial Robustness of Large Vision-Language Models. In *Advances in Neural Information Processing Systems*.
- [45] Hong-Yu Zhou, Xiaoyu Chen, Yinghao Zhang, Ruibang Luo, Liansheng Wang, and Yizhou Yu. 2022. Generalized Radiograph Representation Learning via Cross-supervision between Images and Free-text Radiology Reports. *Nature Machine Intelligence* (2022).